Estimation of atmospheric-pressure non-equilibrium Ar plasma EEDF using optical emission spectroscopy and linear combination of generalized EEDF

W. Kikuchi[1], J. Enomoto[1], K. Yamashita[1], Y. Yamashita[1], A. Nezu[2] and H. Akatsuka[1,2]

[1] *Department of Electrical and Electronic Engineering, Tokyo Institute of Technology, Tokyo, Japan*
[2] *Institute of Innovative Research, Tokyo Institute of Technology, Tokyo, Japan*

Abstract: Using optical emission spectroscopy (OES) measurement and global optimal search methods, the electron energy distribution function (EEDF), electron temperature T_e, and density N_e of dielectric barrier discharge (DBD) atmospheric-pressure non-equilibrium plasma (APNEP) are measured. Continuum emission due to bremsstrahlung is observed to the analysis with the spectrometric system in the visible wavelength range calibrated absolutely. Experimental results are compared with the theoretical spectra determined by linear combination of generalized EEDF in entire measurable range. The methodology to find the best theoretical fitting to obtain the plasma parameters is discussed with global optimization mathematics. It is found that T_e 1.9 – 1.5 [eV] and 0.33 – 0.52 [eV], and the general EEDF parameter γ 11 – 5 and 1 – 2.75 in high- and low- energy regions, respectively, as discharge voltage increases. N_e is confirmed to be approximately 0.63 – 5.3×10^{13}[cm^{-3}].
Keywords: optical emission spectroscopy, global optimal search methods, two-temperature

1. Introduction

Atmospheric-pressure non-equilibrium plasmas (APNEP) have been applied in various fields: modification of material surfaces [1], sterilization [2] and medical treatment because of their low gas temperature and high electron temperature. For further development, their macroscopic characteristic parameters T_e, N_e and electron energy distribution function (EEDF) should be examined by OES measurements, which is more advantageous than Thomson scattering measurements in point of view of cost effectiveness and equipment simplicity for practical application.

OES measurements are performed to observe line and continuum spectra. To analyze the line spectra, collisional-radiative model could be applied. However, it is hard to apply them to the APNEP due to difficulty in the formulation of the excited-state number density and in unique determination in the case of high N_e. On the other hand, the dominant source of continuum radiation is electron–atom bremsstrahlung for the APNEP, and reported that it is available to calculate its T_e and N_e [3 – 4].

Previously, EEDF was reported that it can be described as linear combination of Maxwellian EEDF [5] or single Druvesteynian EEDF in high energy region [6], however it has not been validated by linear combination of generalized EEDF in entire observable range. Furthermore, as later specified, the parameter γ in the analytical formulation in the EEDF is important as well as T_e and N_e because it makes huge difference on the EEDF. To find optimal solutions, global search method and continuum spectrum detection are originally applied, which is precisely the objective of this study.

2. Theoretical analysis

The continuum spectrum mainly consists of recombination radiation and bremsstrahlung for the APNEP. Under atmospheric pressure, if the degree of ionization of the plasma is less than 10^{-3}, the bremsstrahlung due to electron–atom interaction is dominant in the continuum spectrum [3 – 4]. Therefore, the spectral emission coefficient ε_{ea}, which is calculatable by the following equation [4]:

$$\varepsilon_{ea} = \sqrt{\frac{2}{m_e}} \frac{N_e N_a}{\lambda^2} \frac{hc}{4\pi} \int_{\frac{hc}{\lambda}}^{\infty} Q_{ea}^{B}(\lambda, E) \sqrt{E} f(E) \mathrm{d}E \qquad (1)$$

where m_e, N_a, λ, E, Q_{ea}^{B} and $f(E)$ are the electron mass, atom density, wavelength, electron energy, the cross-section of bremsstrahlung due to electron–atom impact, electron energy and general EEDF [7 – 8], respectively. In this study, the EEDF is assumed to be formulated as follows [7 – 8]:

$$f(E) = \gamma \frac{\Gamma\left(\frac{5}{2\gamma}\right)^{\frac{3}{2}}}{\Gamma\left(\frac{3}{2\gamma}\right)^{\frac{5}{2}}} \frac{\sqrt{E}}{\left(\frac{3}{2} k T_e\right)^{\frac{3}{2}}} \exp\left\{ -\left(\frac{\Gamma\left(\frac{5}{2\gamma}\right)}{\Gamma\left(\frac{3}{2\gamma}\right)} \frac{E}{\frac{3}{2} k T_e} \right)^{\gamma} \right\} \qquad (2)$$

In order to optimize the fitting procedure of experimental results with theoretical continuum spectra, deterministic extraction of continuum spectral data from the ones observed experimentally must be accomplished. Hence, a numerical program was coded to perform interpolation recursively between relative minima compared to multiple points in the neighbourhoods.

3. Experiment

Figure 1 shows a schematic overview of the DBD APNEP generator in this experiment. Further details are described elsewhere [6].

The Ar gas flow rate is adjusted with a flow controller and set to 4 L/min to ensure the stability of the discharge. Discharge voltage is applied with a high-voltage power supply as an inverter-type neon transformer, up to 9.0

kV_{p-p} as AC 20 kHz. In the present study, the output voltage V_o was set as 2.7 – 8.1 kV in 0.45 kV steps. A spectrometer (MS3504, SOL Instruments Ltd., Czerny-Turner mount, focal length 350 mm, *F*/3.8, used grating 1200 grooves/mm, blaze wavelength 500 nm) is connected to the optical fiber guide tube. The wavelength sensitivity was calibrated in advance using a standard irradiance light source and a white diffuse reflection element for converting it to a radiance standard. However, this measurement was performed without long-pass filter, and consequently, it may be mixed by higher-order diffraction light.

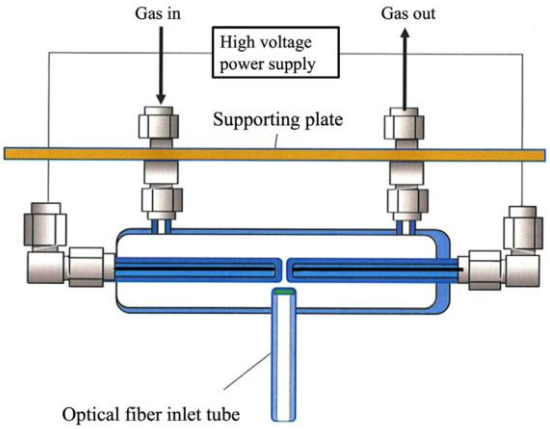

Fig. 1. Schematic diagram of this experimental setup [6].

4. Results and discussion

Comparison between experimental spectral emission coefficient ε_{ea} and theoretical value calculated by Eq. (1) is performed by global search method DIRECT [9] implemented in "SciPy", which is a module of python. To improve the calculation speed and accuracy, the data comparison is processed not for whole observed wavelength region, but separately treated as two wavelength regions. Namely, the "short wavelength" is defined to be the one shorter than 500 nm, while the "long wavelength" is to be longer than 550 nm, Generally, the "short wavelength" corresponds to the high-energy tail region in the EEDF, while the "long wavelength" to the low-energy bulk region of the EEDF [5].

First concerning V_o dependence, different dependence between the short and long range is confirmed. In the short-wavelength range, N_e becomes higher as V_o increases, however T_e and γ become lower as V_o increases. Figure 3 shows the electron energy probabilistic functions (EEPFs). In the long-wavelength range, N_e becomes higher as V_o higher however low V_o is exception, and T_e and γ become higher as V_o increases in a region V_o is 4.5 kV or less. Figure 4 shows the EEPFs. Considering T_e and γ dependence on V_o in both regions, these parameters are getting closer as V_o. Hence this may be caused by relaxation of N_e increases.

Finally, let us discuss the difference between short- and long-wavelength regions in each V_o. There is approximately 10^5 times difference between their N_e. Hence the long-wavelength N_e is dominant in this plasma, which means that the effective T_e averaged with the weight of N_e is close to the "long-wavelength" T_e. However, the "short-wavelength" component has the higher T_e, and consequently, the entire characteristics of the observed APNEP may be different from the one supposed to the plasmas with simply-low mono-temperature T_e.

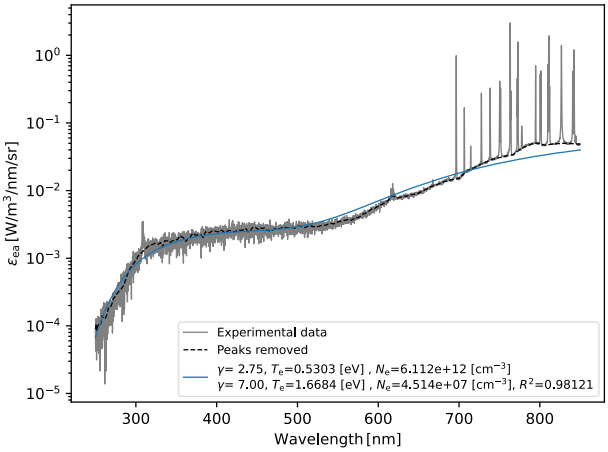

Fig. 2. Best-fitted result when discharge voltage is 4.5kV

Table 1. Optimized result

V_o [kV]	Short wavelength			Long wavelength		
	T_e [eV]	N_e[cm^{-3}]	γ	T_e [eV]	N_e[cm^{-3}]	γ
2.7	1.9	3.9×10^7	11	0.33	5.3×10^{13}	1
3.6	1.8	2.6×10^7	10	0.47	6.3×10^{12}	2
4.5	1.7	5.3×10^7	7	0.47	1.9×10^{13}	2.25
5.4	1.7	6.0×10^7	8	0.52	1.5×10^{13}	2.75
6.3	1.5	1.2×10^8	6	0.52	2.5×10^{13}	2.75
7.2	1.6	9.6×10^7	7	0.52	2.1×10^{13}	2.75
8.1	1.5	2.0×10^8	5	0.52	2.8×10^{13}	2.75

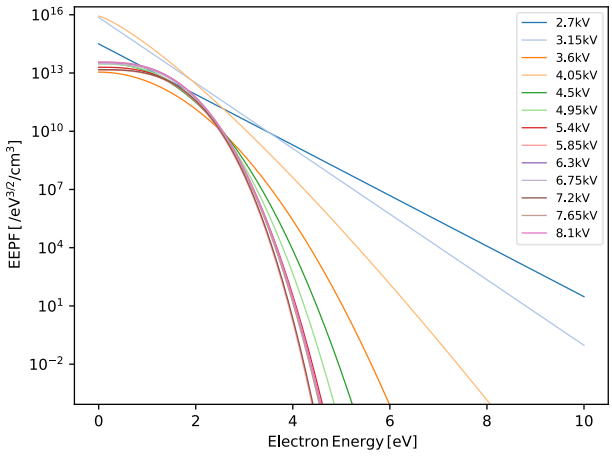

Fig. 3. "Long wavelength" component in the optimized EEPF, which can be considered as its bulk region.

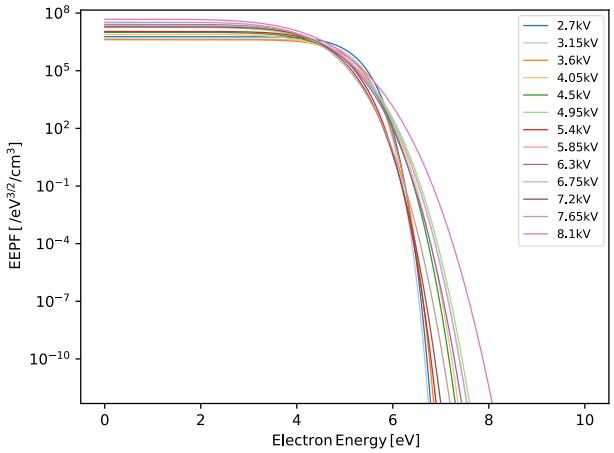

Fig. 4. “Short wavelength” component in the optimized EEPF, which can be considered as its high-energy tail.

5. References

[1] T. Yuji and Y.-M. Sung, *IEEE Trans. Plasma Sci.* **35**, 4, 1010-1013 (2007).

[2] T. Yuji, K. Nakabayashi, H. Kinoshita, N. Mungkung, Y. Suzaki, S. Mamat and H. Akatsuka, *Journal of Food Quality* **2021**, 8896716 (2021).

[3] S. Park, W. Choe, S.Y. Moon, and J. Park, *Appl. Phys. Lett.* **104**, 084103 (2014).

[4] K. T. A. L. Burm, *Plasma Sources Sci. and Technol.* **13**, 387 (2004).

[5] T. van der Gaag, A. Nezu and H. Akatsuka, *Jpn. J. Appl. Phys.* **61**, 076004 (2022).

[6] H. Onishi, F. Yamazaki, Y. Hakozaki, M. Takemura, A. Nezu, and H. Akatsuka, *Jpn. J. Appl. Phys.* **60**, 026002 (2021).

[7] J. T. Gudmundsson, *Plasma Sources Sci. Technol*. **10** 76 (2001).

[8] J. B. Boffard, R. O. Jung, C. C. Lin, and A. E. Wendt, *Plasma Sources Sci. Technol.* **19**, 065001 (2010).

[9] J. M. Gablonsky, and C. T. Kelley, *J. Glob. Optim.* **21**, 27-37 (2001).